RGB-D Scene Recognition with Object-to-Object Relation

Xinhang Song
[1]Key Lab of Intel. Inf. Proc., Inst. of Comput. Tech., Chinese Academy of Sciences, Beijing, 100190, China
[2]University of Chinese Academy of Sciences, Beijing, China
xinhang.song@vipl.ict.ac.cn

Chengpeng Chen
[1]Key Lab of Intel. Inf. Proc., Inst. of Comput. Tech., Chinese Academy of Sciences, Beijing, 100190, China
[2]University of Chinese Academy of Sciences, Beijing, China
chengpeng.chen@vipl.ict.ac.cn

Shuqiang Jiang
[1]Key Lab of Intel. Inf. Proc., Inst. of Comput. Tech., Chinese Academy of Sciences, Beijing, 100190, China
[2]University of Chinese Academy of Sciences, Beijing, China
sqjiang@ict.ac.cn

ABSTRACT

A scene is usually abstract that consists of several less abstract entities such as objects or themes. It is very difficult to reason scenes from visual features due to the semantic gap between the abstract scenes and low-level visual features. Some alternative works recognize scenes with a two-step framework by representing images with intermediate representations of objects or themes. However, the object co-occurrences between scenes may lead to ambiguity for scene recognition. In this paper, we propose a framework to represent images with intermediate (object) representations with spatial layout, i.e., object-to-object relation (OOR) representation. In order to better capture the spatial information, the proposed OOR is adapted to RGB-D data. In the proposed framework, we first apply object detection technique on RGB and depth images separately. Then the detected results of both modalities are combined with a RGB-D proposal fusion process. Based on the detected results, we extract semantic feature OOR and regional convolutional neural network (CNN) features located by bounding boxes. Finally, different features are concatenated to feed to the classifier for scene recognition. The experimental results on SUN RGB-D and NYUD2 datasets illustrate the efficiency of the proposed method.

KEYWORDS

Intermediate representation; spatial layout; object detection; RGB-D; scene recognition

1 INTRODUCTION

The goal of scene recognition is to annotate images with scene categories. Humans have innate talent to recognize those abstract scenes without hard training, while it is typically challenging for computer, since most scenes are abstract representations composed of many less abstract entities in local regions (e.g. water, wall, people, chairs), which require reasoning from digital pixels to the abstract scenes. Scene categories can be inferred from low-level visual descriptors[29, 31, 40, 41], with the "bag" model of local visual descriptors. However, it's difficult to obtain the required statistical knowledge for inferring scene categories from low-level visual features, due to the semantic gap [36].

An alternative approach is to split the scene reasoning in two steps with smaller semantic gap (including pixels to objects, objects to scenes), with the intermediate representations, such as object banks[23], latent topic models[4, 11, 24, 25, 27], mid-level parts[21] and regional (in multi-scale) features of convolutional neural network (CNN) [6, 16]. However, due to the object co-occurrences between different scenes, only representing images with such intermediate representations suffers from the problem of ambiguity for recognizing scenes.

A more discriminative approach is to represent images by intermediate representations with spatial layout. Spatial layout is helpful to distinguish some particular scenes that are confused by intermediate presentations (see Fig. 1, different scenes such as "dining room" and "classroom" may contain similar objects like "table" and "chair". When only using the intermediate representations, the images of those two categories are difficult to be distinguished. However, when considering the intermediate representations with spatial layout, those scenes can be distinguished, i.e., in "dining room", the table is usually *surrounded* by the chairs, while in "classroom" the chairs are always *behind* the "table").

One intuitive way to obtain both intermediate representations and spatial layout is using object detection techniques [14, 15, 28], which can simultaneously provide object labels and the position of their bounding boxes. The intermediate representations are built on the statistical histogram of objects, and the spatial layout is analyzed by the position (coordinates) of the predicted bounding boxes. Particularly, some previous works [2, 13, 39] have implemented object detection techniques for scene recognition. However, these works either only use the object labels but not the spatial information [2, 13], or only locate the position of bounding boxes to extract local features [39] while ignore the object labels.

Particularly, the RGB-D data is helpful to better locate the objects. The low cost depth sensors, such as Microsoft Kinect, can capture RGB-D data, which extends traditional RGB recognition by including depth information. Depth camera can provide spatial information to detect object boundaries and understand the global layout of objects in the scene. Combining RGB with depth images to recognize scenes usually achieves better performance than only using RGB or depth images. Previously, depth information is modeled using handcrafted features. Although automatic feature learning from the data with CNN can provide more discriminative representations, however, the lack of large RGB-D datasets makes the complex CNN models not applicable. Recently, Song *et al.* [33]

MM '17, October 23–27, 2017, Mountain View, CA, USA.

ACM ISBN 978-1-4503-4906-2/17/10…$15.00
https://doi.org/10.1145/3123266.3123300

Figure 1: Scenes "dinning room" and "classroom" have similar objects co-occurrence, but different spatial layout. Here, intermediate representation such as object distribution may not be discriminative enough to distinguish these two scenes, while including spatial layout is more helpful.

proposed SUN RGB-D, a larger scene RGB-D dataset that can be used to train more complex models.

In this paper, we propose a framework for scene recognition, where the intermediate representations with spatial layout are extracted on the RGB-D multi-modal data to address the ambiguous problem caused by object co-occurrences between scenes. In the proposed framework, the object detection technique is adapted to the RGB-D multi-modal data. First, the regional proposals (bounding boxes) are detected separately from RGB and depth data, then merged by the proposed RGB-D proposal process. Later, the detected results are used to build object-to-object relation (OOR) representation, which represents images with both intermediate categories and their relative relations. Meanwhile, the detected bounding boxes are also used for locating the regions to extract local CNN hidden features, and the whole images are fed to CNN to extract the global features. Finally, local and global CNN feautures are combined by training an extended multi-layer network, and the combined CNN features are concatenated with OOR to feed to classifier for scene recognition.

2 RELATED WORK

2.1 Intermediate representation

Vogel and Schiele [38] proposed to represent natural scenes with regional intermediate representation of local concepts such as *water*, *rocks* or *foliage*. Similarly, Object bank [23] trains classifiers with multi-scale images from ImageNet to obtain a more descriptive representation. The *classemes* representation[3] is based on a set of fixed basis classes. Attributes[10, 22] follow a similar idea, where classifiers are trained to detect whether certain attributes are present or not. Attributes can be modeled at both local and global levels, and defined for both objects[10] and scenes[26]. However, without exact object detection, the intermediate representation is not that reliable to obtain good performance for scene recognition.

2.2 Object detection

By leveraging the successful deep neural networks from object classification, Girshick *et al.* [15] propose an R-CNN framework for object detection, which aggregates the region proposal technique [37] with CNN classifier. Although R-CNN improves the previous works [7, 12] with a large margin in accuracy, the repeated CNN feature extraction (for each proposal) still limits R-CNN for efficiency. Thus, Girshick *et al.* [14] propose the Fast R-CNN framework to improve the R-CNN with ROI pooling layer and multi-task regression layer. The former accelerates R-CNN by pooling on feature maps rather than image pixels, which only requires the CNN feature extraction once for all the proposals of one image. The later jointly train the object classifiers and bounding boxes regressor. While, this Fast R-CNN still relies on the external region proposal mechanism. Recently, Ren *et al.* [28] propose the Faster R-CNN framework to address the region proposal problem with a region proposal network (RPN), which establishes the end-to-end training for object detection.

More recently, some works [2, 13, 39] have implemented object detection technique for scene recognitions. George *et al.* [13] propose to represent scene images by object distributions based on object detection, which is then optimized to distinguish fine-grained scenes by semantic clustering. Bappy *et al.* [2] combines object detection with manual annotation for active learning of scene recognition. Only representing images with object distributions lacks of spatial information. Wang *et al.* [39] extract local features located by the object detection, and local features are embedded with Fisher Vector.

In this paper, we leverage both object distributions and spatial information to represent images for scene recognition.

2.3 RGB-D recognition

Handcrafted features [1, 18] are engineered to capture some specific properties that the engineer has observed to be useful for RGB-D image recognition. Also, Socher *et al.* [32] use a single layer CNN trained on patches. The network is learned in an unsupervised way, and then combined with a recurrent convolutional network (RNN). After the availability of large datasets, the interest has shifted towards deep networks pretrained with RGB data from ImageNet or Places, which have shown better performance than previous smaller CNN models [19, 35]. Gupta *et al.* [19] use R-CNN on depth images to detect objects in indoor scenes. In order to address the problem of limited training data, they augment the training set by rendering additional synthetic scenes.

Fine-tuning or transferring the RGB pretrained CNN models to depth data are proposed in recent works [20, 39, 43]. Wang *et al.* [39] fine-tune the pretrained CNN with depth images, and extract

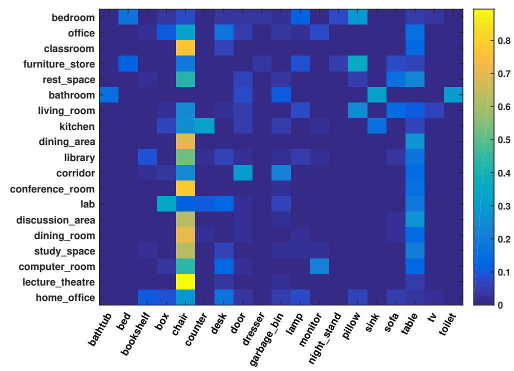

(a)

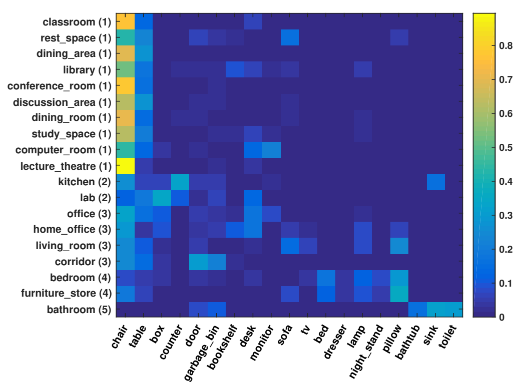

(b)

Figure 2: Co-occurrences between objects and scenes, (a) correlation matrix, (b) correlation matrix after reordering with clustering, where the "(#)" represents the cluster ID.

features on both local regions and whole images, then combine all features of RGB and depth patches/images in a component aware fusion method. Zhu *et al.* [43] jointly fine-tune the RGB and depth CNN models by including a multi-model fusion layer, simultaneously considering inter- and intra-modality correlation, meanwhile regularizing the learned features to be compact and discriminative. Alternatively, Gupta *et al.* [20] propose to transfer RGB CNN model to the depth data according to the RGB and depth image pairs. While Song *et al.* [34] do not depend on fine tuning or transferring, they train CNN with depth patches by weak-supervision, which achieves even better performance than fine tuning from RGB.

3 IMAGE REPRESENTATIONS BASED ON CONTENT RELATION

We first introduce the proposed intermediate representations with spatial layout, and then compare different types of image representations based on object distributions.

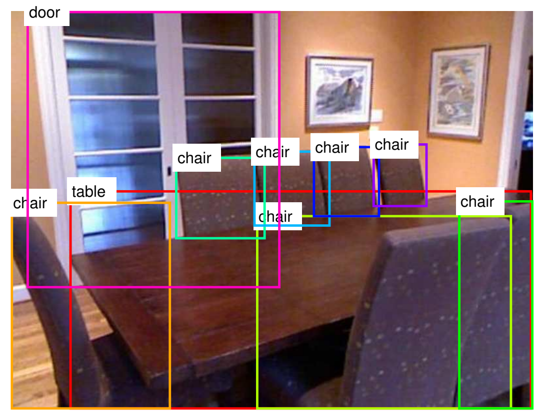

(a) "dinning room"

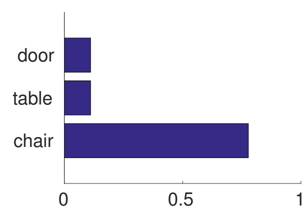

(b) P^I_O

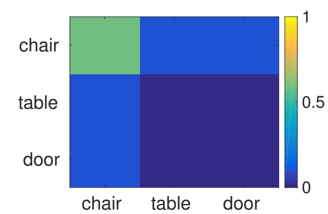

(c) P^I_{OO}

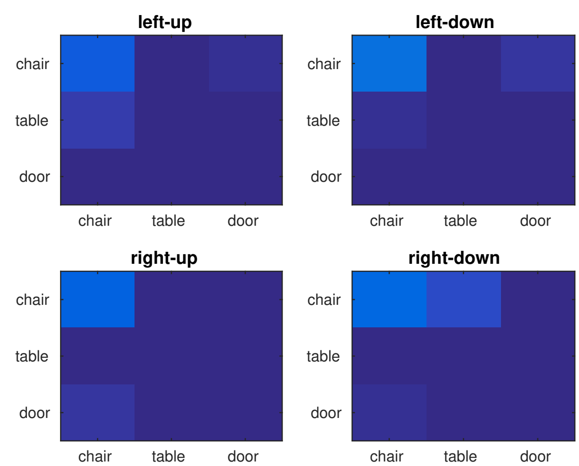

(d) P^I_{OOR}

Figure 3: Feature visualization of a toy example, (a) one image of "dinning_room" from SUN RGB-D, and the object annotations are from the ground truth, (b) the visualization of P^I_O, which is normalized by the counting of appearances, we select 3 object categories for this toy example (c) the visualization of P^I_{OO}, the counting of object co-occurrences, (d) the visualization of P^I_{OOR}, 4 types of relative relations between the centers of object bounding boxes are selected here, i.e., the "left-up" means the co-occurrences between objects with such relation. Note that (c) and (d) are the visualizations of feature, and for training classifiers, the features are stretched to vectors.

3.1 Object-to-object relation representation

The common intermediate representations are object distributions, which can be represented as $P_O^I = \left[p_1^I, p_2^I, \ldots, p_{|O|}^I\right]$ (see Fig. 3b), where p_i^I is the appearance frequency of object i observed in the image I, and O is the object vocabulary. With this type of representation, the object co-occurrences between scenes may confuse the recognition. A more discriminative way is representing images with object-to-object co-occurrences, $P_{OO}^I = \begin{bmatrix} p_{11}^I & \cdots & p_{1|O|}^I \\ \vdots & \ddots & \vdots \\ p_{|O|1}^I & \cdots & p_{|O||O|}^I \end{bmatrix}$ (also see Fig. 3c), where each element p_{ij}^I represents the appearance frequency of co-occurrence between object i and j.

The proposed intermediate representation is composed of objects and relative relations, which is represented as the triplet $\langle object, relation, object \rangle$, also denoted as object-to-object relation (OOR) representation. The proposed OOR can be formulated as a tensor $P_{OOR}^I \in R^{|O| \times |V| \times |O|}$ (see Fig. 3d), where V is the vocabulary of relative relations between objects. Particularly, we define the relative relations based on the coordinates of object bounding boxes $b = [x_l, y_u, x_r, y_d]$, where $[x_l, y_u]$ is left-top corner, and $[x_r, y_d]$ is the right-down corner. The relation between object i and j are represented as

$$\begin{aligned} V(i,j) &= \left[f\left(b^i - b^j\right)\right] \\ &= \left[f\left(x_l^i - x_l^j\right), f\left(y_u^i - y_u^j\right), f\left(x_r^i - x_r^j\right), f\left(x_d^i - x_d^j\right)\right] \end{aligned} \tag{1}$$

,

where $f(x) = \begin{cases} 0, & if \quad x <= 0 \\ 1, & if \quad x > 0 \end{cases}$. There are $|V| = 2^4 = 16$ different types of relative relations between objects.

3.2 Insights of OOR representation

We analyze the problem of object co-occurrences between scenes, and compare the proposed OOR with others on the SUN RGB-D [33] dataset. This dataset contains 40 categories with 10335 RGB-D images. Following the publicly available split in [33, 39], 19 most common categories are selected, consisting of 4,845/4659 images for training/test. Also, 19 popular object categories are selected in [33] for the object detection, whose annotations are given with the bounding box coordinates and object labels.

3.2.1 Object co-occurrences between scenes. We illustrate the statistics of the co-occurrences (appearing in the same image) between objects and scenes in a correlated matrix W, which is visualized in Fig. 2a. Each element W_{so} in the matrix is the co-occurrence frequency between scene s and object o. With such matrix W and the object distributions P_O^I, the scene probability distribution can be obtained as:

$$P_S^I = P_O^I W^\mathsf{T} \tag{2}$$

With P_S^I, we can predict the scene label by finding the scene category with maximum probability. Also, the scene label can be predicted by training SVM classifiers based on the representations of P_O^I, P_{OO}^I, and P_{OOR}^I.

3.2.2 Insights in the analysis of confusion. Confusion matrixes of different representations are compared in the Fig. 4, where the accuracy is calculated by the mean of diagonal. Note that the accuracy of P_S^I (Fig. 4a) is much lower than others. Particularly, many scenes such as "dining area", "conference room" and "dining room" are misclassified to "classroom". This confused problem is mainly caused by similar object co-occurrences among these scenes. In order to better visualize such confusion between scenes, the correlation matrix in Fig. 2a is re-organized with the spectral clustering [5] algorithm. The Fig. 2b visualizes the correlation matrix after re-ordering the rows and columns. In practice, the number of cluster is $k = 5$, the scenes (rows) are reordered by the cluster ID, and the objects (columns) are reordered according to the correlation to the scenes. It can be observed that many scene categories such as "classroom", "dining area", "dining room", and "conference room" are clustered together because of the co-occurring of objects like "chairs" and "tables" (see the first two columns in Fig. 2b), this is also the reason of the confusion between scenes in Fig. 4a.

Rather than using Eq. 2 to predict scene labels, we also recognize scenes with SVM classifier on different types of object representation of P_O^I, P_{OO}^I, and P_{OOR}^I, whose confusion matrixes are visualized in Fig. 4b-d. The results of Fig. 4a and b are based on the same object representation P_O^I, but using different classifiers, i.e., Eq. 2 and SVM. The comparison between them shows the efficiency of more discriminative classifier SVM. Moreover, using P_{OOR}^I with SVM (in Fig. 4d) results even better performance than P_O^I and P_{OO}^I, including better overall accuracy and less confused problems in the confusion matrix. For instance, the confusion between "classroom" and "dinning room" in Fig. 4d is much better than that in Fig. 4a, where the rate of misclassifying from "dinning room" to "classroom" gets lower from 87% to 20%. This also supports our hypothesis (in Fig. 1) that the scenes with object co-occurrences also can distinguished by including the relative relations into the intermediate representation.

The above evaluations are based on the ground truth of annotated objects. While for the real world scene recognition, the annotations of object are not available. Thus, we implement object detection technique to obtain the labels and bounding boxes of objects, which will be introduced in next section.

4 DETECTION OF IMAGE CONTENT

In order to include object information for more accurate scene recognition, we apply object detection technique on each image, and represent the images with features based on the detected results. In particular, we adapt Faster R-CNN model [28] to the RGB-D data, and the RGB and depth modalities are combined at proposals generating process, more details are introduced in this section.

4.1 RGB-D object detection

Being a region based method for object detection, Faster R-CNN includes a branch, named region proposal network (RPN), to generate candidates of bounding box. On each candidate region, the CNN hidden features are first extracted by region of interest (RoI) pooling layer, then fed to the classifying layers, which consist of two clssifiers, a softmax classifier for object labels and a regressor for the coordinates of bounding box.

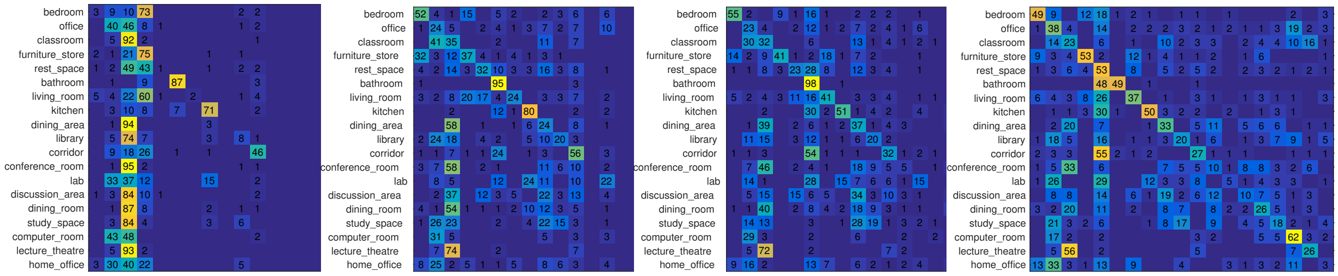

(a) Accuracy: 22.8% (b) Accuracy: 28.1% (c) Accuracy: 28.8% (d) Accuracy: 31.1%

Figure 4: Confusion matrix, evaluated with annotated objects from ground truth, (a) P_S^I in Eq. 2, (b) P_O^I with SVM, (c) P_{OO}^I with SVM, (d) P_{OOR}^I with SVM.

In this work, we separately train two Faster R-CNN models on RGB and depth data, and denote them as FRCN-RGB and FRCN-Depth, respectively, where ZF net [42] is used as pre-trained model in the training process.

Besides, in order to combine RGB and depth modalities, we train a new model after combining those two models, named FRCN-RGBD, to take advantages of both modalities. In FRCN-RGBD, two branches of CNN architectures (copied from FRCN-RGB and FRCN-Depth, respectively) are followed by three fully-connected layers and one softmax layer. Recalling the RPN in Faster R-CNN model, it shares convolutional layers with the detection network. In our case, the FRCN-RGBD contains two RPNs from FRCN-RGB and FRCN-Depth, which generate proposals independently. In order to combine RGB and depth models, we establish a RGB-D fusion method on these two independent sets of region proposal . Our fusion method consists of two steps, including RGB-D proposal fusion and proposal refinement with non-maximum suppression (NMS) [28].

4.2 RGB-D proposal fusion

With the RPN branches, the proposals $B_{rgb} = \left\{B_{rgb}^{(1)}, \ldots, B_{rgb}^{(n)}\right\}$ and $B_{depth} = \left\{B_{depth}^{(1)}, \ldots, B_{depth}^{(n)}\right\}$ are obtained on each pair of RGB and depth images, where each $B_{rgb}^{(i)}$ and $B_{depth}^{(i)}$, $i = [1, \ldots, n]$, contain the proposal information in form of bounding box, including the coordinates $b_{rgb}^{(i)}$, $b_{depth}^{(i)}$ and confidence score $C_{rgb}^{(i)}$ and $C_{depth}^{(i)}$. Let $N_{rgb}^{(i)}$ and $N_{depth}^{(i)}$ be the number of proposals contained in $B_{rgb}^{(i)}$ and $B_{depth}^{(i)}$, respectively. Besides, we set

$$N_{rgb}^{(i)} = min\left\{\left|C_{rgb}^{(i)} > \alpha\right|, \lambda\right\}$$

$$N_{depth}^{(i)} = min\left\{\left|C_{depth}^{(i)} > \alpha\right|, \lambda\right\}$$

Where $\left|C_{rgb}^{(i)} > \alpha\right|$ denotes the number of proposals with value $C_{rgb}^{(i)}$ larger than α, which is considered as the confidence threshold, and λ is an empirical value of the minimal number of proposals, ensuring enough proposals. The hype-parameters α and λ are evaluated in the following section. Note that these two hype-parameters α and λ decide the top $N_{rgb}^{(i)}$ ($N_{depth}^{(i)}$) proposals selected from $B_{rgb}^{(i)}$ ($B_{depth}^{(i)}$) based on $C_{rgb}^{(i)}$ ($C_{depth}^{(i)}$).

Intuitively, the proposals obtained from RGB and depth models should be combined to improve the detection performance. By directly combining the proposals of $B_{rgb}^{(i)}$ and $B_{depth}^{(i)}$, we get $B_{rgbd}^{(i)} = \left[B_{rgb}^{(i)} \cup B_{depth}^{(i)}\right]$. However, it is unavoidable to lead to the overlapping between $B_{rgb}^{(i)}$ and $B_{depth}^{(i)}$, making the features of overlapping region redundant for further scene recognition task. To avoid overlapping, a pooling process on bounding boxes level is performed on these proposals. Particularly, NMS is applied to get the pooled proposals $B_{pooled} = \left\{B_{pooled}^{(1)}, \cdots, B_{pooled}^{(n)}\right\}$, in which

$$B_{pooled}^{(i)} = NMS\left\{B_{rgb}^{(i)} \cup B_{depth}^{(i)}, \beta\right\}$$

where β is the Intersection-over-Union (IoU) overlapping threshold for non-maximum suppression. That means the regions with relatively overlapping area larger than β will be merged.

5 MULTI-MODAL SCENE RECOGNITION

Some previous RGB-D works [33, 34, 43] recognize scene by training the CNN models with images, and extracting global features of CNN activation (e.g., fc7 or fc8) based on the whole image. While an alternative is to extract local features with object detection [39], and the local and global features are combined with Fisher Vector encoding. In [39], the object detection is mainly used for locating the regions and extracting features, while the object labels are ignored. Thus, besides extracting the local and global hidden features of CNN activation, we also learn OOR representation P_{OOR}^I. All these features (hidden features of CNN activation and semantic features OOR) are concatenated to feed to the classifier of scenes.

Multi-modal global features. Rather than the very deep and complex architectures, Song *et at.* [34] propose a relatively shallow and simple architecture for depth data that trained with weak-supervision. Then the authors concatenate depth and RGB CNNs with fully connected layers. In order to extract multi-modal global features, we apply the DCNN model in [34] to extract depth features, and combine RGB and depth data with RGB-D-CNN in [34].

Table 1: Object detection AP (%) of SUN RGB-D

Model	bathtub	bed	bookshelf	box	chair	counter	desk	door	dresser	garbage_bin
FRCN-RGB	34.4	63.2	39.8	12.5	43.9	42.2	20.3	30.7	30.0	40.0
FRCN-Depth	54.5	71.6	25.5	5.0	45.4	39.5	22.2	10.5	18.0	34.2
FRCN-RGBD	**57.5**	**75.6**	**44.2**	**17.7**	**49.6**	**48.9**	**25.4**	**33.6**	**40.2**	**49.2**
Model	lamp	monitor	night_stand	pillow	sink	sofa	table	tv	toilet	mAP
FRCN-RGB	38.5	34.3	39.2	33.0	46.9	39.5	34.6	23.2	74.5	37.9
FRCN-Depth	40.0	18.8	34.8	40.2	49.2	44.9	41.2	14.3	70.0	35.8
FRCN-RGBD	**53.0**	**44.0**	**47.6**	**48.6**	**61.1**	**50.3**	**43.2**	**35.2**	**81.7**	**47.7**

Multi-modal local features. After obtaining the region proposals with RPN, the local features of CNN (fc7) activation are extracted within the bounding box of each proposal. For the multi-modal local features, the proposals are separately detected from each modality, and then combined together with the fusion process in Section 4.2. For one image, the local features of all the proposal are combined into a global feature by max pooling process, which is then fed to train the scene classifiers. Note that the OOR representation is different to this local feature, since the object detection here is mainly used for locating the regions with detected bounding boxes.

Multi-modal multi-feature combination. The global and local features are extracted from CNN activation, which are further combined with an extended multi-layer network, training with the loss of scene labels. Thus, the local and global CNN features are combined to a global CNN feature, which is then concatenated with OOR to include the spatial layout information of image content (objects). Finally, the concatenated features are fed to the SVM classifier for scene recognition.

6 EXPERIMENTS

6.1 Setting

Dataset. Our approaches are evaluated on two datasets: NYU Depth Dataset version 2 (NYUD2) [30] and SUN RGB-D[33]. The former consists of 27 indoor categories. Following the original training/test split of images 795/654 in [30], all 27 categories are reorganized into 10 categories, where some of categories with few images are combined into a joint category "other". The latter contains 10335 RGB-D images in 40 categories,. Following the public split in [33, 39], the 19 most common categories are selected, consisting of 4,845/4659 images for training/test. The split is provided in the toolbox of SUN RGB-D dataset. For the object detection evaluation, we follow the same split of scene recognition, since the object detection further serves for the scene recognition. All depth images are encoded to HHA images using the code in [19].

Classifier . We optionally use class-specific weights (weight is an option implemented in liblinear[9]) to compensate the imbalance in training data. The weight $w = \{w_1 ... w_M\}$ of each category m is computed as $w_m = (\min_{i \in M} N_i \setminus N_m)^p$, where N_m is the amount of training images of the m^{th} category. We practically set $p = 1$.

Evaluation metric. Following [33, 39], we report the average class accuracy for the scene recognition. We follow the evaluation method of [8] to report the average precision (AP) for object detection. Detected results are considered to be true or false positives according to the overlap area with ground truth bounding boxes. To be considered a correct detection, the overlap area a_o between the predicted bounding box B_p and ground truth bounding box B_{gt} must exceed 50% by the formula:

$$a_o = \frac{area\left(B_p \cap B_{gt}\right)}{area\left(B_p \cup B_{gt}\right)}$$

6.2 Object detection

6.2.1 Implementation . For the object detection model training, both FRCN-RGB and FRCN-Depth use the ZF net [42] as the pretrained model, and follow the empirical parameter setting of Faster RCNN.

For the training of FRCN-RGBD model, all the convolutional layers are copied from FRCN-RGB and FRCN-Depth, and the hidden layer outputs of the region proposals $B^{(i)}_{pooled}$ are concatenated to further train the new fully-connected and loss layers. The weights of the previous models are used for initializing the corresponding new layers, which speeds up model training significantly. Particularly, since the concatenation of the outputs of hidden layers results double amount of weights between the concatenated layer and the first fully-connected layer, the corresponding weights of FRCN-RGB and FRCN-Depth are concatenated for the initialization as well, while those weights are divided by 2 to avoid activation saturation. For the other two fully-connected layers, the sizes of weight are as same as that in FRCN-RGB and FRCN-Depth. Here, we take the average of weights from both models to initiate those two fully-connected layers of FRCN-RGBD model. With such trick of weights initialization, the model converges in a few thousand iterations.

For the object detection task, we set $\lambda = 200$ for both FRCN-RGB and FRCN-Depth models, and $\alpha = 0.3$, $\beta = 0.6$ following the empirical setting of Faster RCNN work. Note that this setting is only used for object detection. For the scene recognition task, we practically find the best parameters.

6.2.2 Detection performance. We evaluate the performance of object detection on SUN RGB-D dataset, and the comparisons between different models of different modalites are illustrated in Table 1. Comparing between RGB and depth modalities, depth model works better on the object categories such as "bathtub", "bed", "chair", "pillow" and "table", that contain enough depth information in shapes, while works much worse than RGB model on that objects such as "door", "dresser", "monitor", "tv", that barely have depth in shapes (thin and flat in shape). However, with the RGB and depth fusion, the performances of all category are improved,

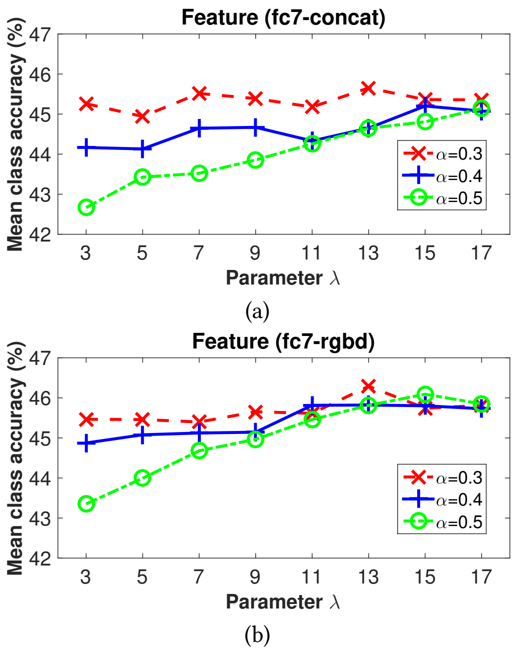

Figure 5: Parameter evaluation of object detection for scene recognition, evaluated on the SUN RGB-D dataset, (a) $F_{fc-concat}$, concatenation of fc7 activation of FRCN-RGB and FRCN-Depth, (b) $F_{fc-rgbd}$, fc7 activation of FRCN-RGBD.

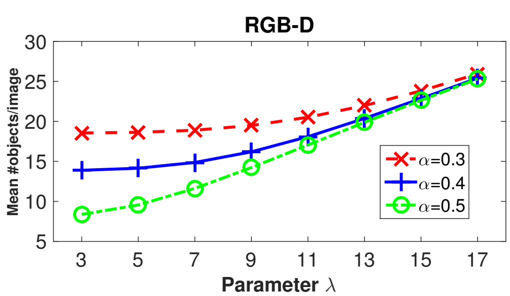

Figure 6: Average number of objects detected from each image on SUN RGB-D.

and the overall result (mAP) of RGB-D model outperforms RGB and depth models with a large margin about 10%.

6.3 Scene recognition

6.3.1 Parameter evaluation of object detection for scene recognition. For the scene recognition, the detected information of objects are used for feature extraction. We first obtain region proposals with RPN, then extract fc7 (last but one fully-connected layer) activation for each proposal, and finally the regional fc7 activation are combined to a global feature vector by max pooling on all proposals from one image. With FRCN-RGBD model, the combined feature is denoted as $F_{fc-rgbd}$. For comparison, we also consider another way of RGB-D fusion. For each image, we concatenate activation from FRCN-RGB and FRCN-Depth models to get a 8192-dimensional (two fc7 4096-dimensional activation) feature vector, denoted as $F_{fc-concat}$. Besides, to speed up classification model training, the general dimension reduction method PCA, is perform on $F_{fc-concat}$ and $F_{fc-rgbd}$, which projects them to 512-dimensions. Note that, this dimension reduction process speeds up the classifier training barely with accuracy loss.

The evaluations of parameter α and λ are illustrated in Fig. 5. Note that, for the scene recognition, the larger λ results more overlapped area between proposals, redundant local features and proposals with lower confidence. Thus, we select much smaller λ for scene recognition. For both $F_{fc-concat}$ and $F_{fc-rgbd}$ in Fig. 5 a and b, the smaller α and larger λ lead to better results, and best results are obtained when $\alpha = 0.3$ and $\lambda = 13$. The average number of detected objects of each image are illustrated in Fig. 6. For the larger α (e.g., $\alpha = 0.4$ or $\alpha = 0.5$), it shows that the average number of detected objects obviously increases with λ, which is also the reason of accuracy improvement in Fig. 5, particularly for $\alpha = 0.5$. Based on the selection of best results, we set $\alpha = 0.3$ and $\lambda = 13$ of object detection model for the rest experiments of scene recognition.

Table 2: Scene recognition accuracy (%) with intermediate representation

Intermediate representations	RGB	Depth	RGB-D
P^I_S	16.8	13.9	17.8
P^I_O	31.4	26.5	31.9
P^I_{OO}	32.7	28.7	33.4
P^I_{OOR}	**33.5**	**30.0**	**36.3**

6.3.2 Intermediate representation. We build the intermediate representations of different modalities based on the object detection results. The comparisons between different intermediate representations are illustrated in Table 2. Note that, the main difference between the results in this table and Fig 4 is the source of object labels and their bounding boxes. The intermediate representations of RGB, depth and RGB-D in this Table 2 are based on the detected results of FRCN-RGB, FRCN-Depth and FRCN-RGBD, while the results in Fig. 4 are relied on ground truth annotations. Compared with the intermediate representations in Fig. 4, the P^I_S are much worse due to the lack of confidence for the object detection results. However, the other results of P^I_O, P^I_{OO} and P^I_{OOR} outperform the ones in Fig. 4, especially the ones built on the detected results after RGB-D fusion, obtaining the best result with 36.3%. Comparing with different representations, the P^I_{OOR} achieves best results in each modality, which outperforms P^I_{OO} from 0.8% (RGB) to 2.9% (RGB-D), where the main improvement benefits from the depth data.

6.3.3 Hidden features. The results of scene recognition with local and global features of CNN activation on different modal data

Table 3: Scene recognition accuracy (%) with CNN activation

Feature	RGB	Depth	RGB-D
Local (object)	43.5	40.0	46.3
Global	41.4	41.1	51.5

Table 4: Comparisons on SUN RGB-D in accuracy(%)

	Method	RGB-D
Proposed	Local-OOR	**50.3**
	Global+Local	**52.6**
	Global+Local-OOR	**54.0**
State-of-the-art	Song *et al.* [33]	39.0
	Zhu *et al.*[43]	41.5
	Wang *et al.* [39]	48.1
	Song *et al.* [34]	52.4

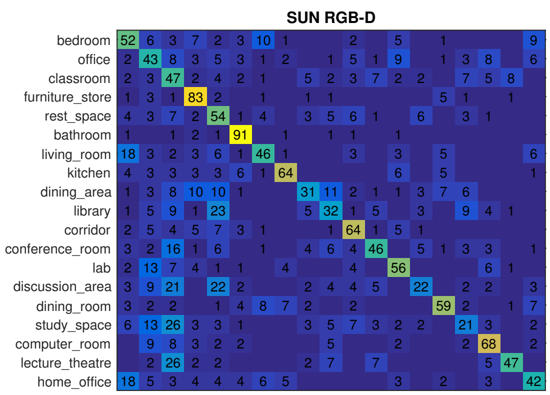

Figure 7: Confusion matrix of Global+Local-OOR.

are illustrated in Table 3. With the RGB and depth multi-modal feature fusion, the RGB-D features outperform single-modal features with the gains 2.8%/10.1% of local/global features in accuracy.

6.3.4 Comparison to the state-of-the-art. Different types of feature are combined to compare with the state-of-the-art works [33, 34, 39, 43], and the comparison results are illustrated in Table 4. Some works [33, 43] only depend on the global features, while Wang *et al.* [39] propose to extract both global features and local features for scene recognition. Although the work of [34] does not explicitly extract local features, the depth model (DCNN) of this work is trained based on local patches with weak-supervision. Somehow, the local information is implicitly included in this work. Based on the object detection results, by concatenating the local feature and OOR representation, our method Local-OOR obtains 50.3% and outperforms the work of [39] more than 2%. Note that the proposed Local-OOR only extracts the local features (OOR is also a kind of local features), while [39] combines both local and global features. Although the single global feature in Table 3 does not work as well as that in [34], by combining local and global features and concatenating with OOR, our Global+Local+OOR achieves the state-of-the-art result with 54.0%, outperforming [34] with 1.6%, also see Fig. 7 for the confusion matrix of Global+Local-OOR. Note that we take fc7 (with 4096 dimension) activation as the global feature, in contrast to the fc8 (with 19 dimension) activation in [34].

Table 5: Comparisons on NYUD2 in accuracy(%)

Method	RGB	Depth	RGB-D
Proposed methods			
Local	51.2	46.4	56.4
OOR	45.1	40.9	48.6
Global	57.3	54.1	64.0
Local-OOR	-	-	60.1
Global+Local-OOR	-	-	**66.9**
State-of-the-art			
Gupta *et al.* [17]			45.4
Wang *et al.* [39]			63.9
Song *et al.* [34]			65.8

6.4 NUYD2

We do not train new CNN models for NYUD2 dataset. Since this dataset contains much less data than SUN RGB-D, we mainly fine tune the pretrained models of SUN RGB-D to the NYUD2. Particularly, the Faster RCNN models of object detection of SUN RGB-D is directly applied to this NYUD2 dataset. Since using RGB-D features obtains much better performance, we mainly report results of RGB-D features of Local-OOR and Global+Local-OOR. Comparing to other works [17, 34, 39], our proposed Global+Local-OOR achieves the state-of-the-art performance of 66.9%.

7 CONCLUSION

Different scenes contain different object co-occurrences, so representing images with object based intermediate representation may result in ambiguity for scene recognition. By analyzing the limitation of intermediate representation, we propose to represent images with objects and their relative relations, i.e., object-to-object relation (OOR) representation. Particularly, we show that OOR representation is more discriminative than object based representation for the scenes with similar object co-occurrences. Meanwhile, in order to better model the spatial information, the OOR is built on RGB-D data. And the depth data is shown to be helpful for both object detection and scene recognition tasks, especially for the objects with depth in shape. However, more discriminative representations with relative relations , the end-to-end training and predicting framework for scene recognition with OOR are also the goals of our future works.

ACKNOWLEDGMENTS

This work was supported in part by the National Natural Science Foundation of China under Grant 61532018 and 61322212, in part by the Beijing Municipal Commission of Science and Technology under Grant D161100001816001, in part by the Lenovo Outstanding Young Scientists Program, in part by National Program for Special Support of Eminent Professionals and National Program for Support of Top-notch Young Professionals. This work was supported by the National Postdoctoral Program for Innovative Talents under Grant BX201700255.

REFERENCES

[1] Dan Banica and Cristian Sminchisescu. 2015. Second-Order Constrained Parametric Proposals and Sequential Search-Based Structured Prediction for Semantic Segmentation in RGB-D Images. In *The IEEE Conference on Computer Vision and Pattern Recognition (CVPR).*

[2] Jawadul H. Bappy, Sujoy Paul, and Amit K. Roy-Chowdhury. 2016. *Online Adaptation for Joint Scene and Object Classification.* Springer International Publishing, Cham, 227–243. DOI: https://doi.org/10.1007/978-3-319-46484-8_14

[3] Alessandro Bergamo and Lorenzo Torresani. 2014. Classemes and Other Classifier-based Features for Efficient Object Categorization. In *IEEE Trans. on Pattern Anal. and Mach. Intell.*

[4] A. Bosch, A. Zisserman, and X. Muoz. 2006. Scene classification via pLSA. In *ECCV*, Vol. 4. 517–530.

[5] Inderjit S. Dhillon. 2001. Co-clustering Documents and Words Using Bipartite Spectral Graph Partitioning. In *Proceedings of the Seventh ACM SIGKDD International Conference on Knowledge Discovery and Data Mining (KDD '01).* ACM, New York, NY, USA, 269–274. DOI: https://doi.org/10.1145/502512.502550

[6] Mandar Dixit, Si Chen, Dashan Gao, Nikhil Rasiwasia, and Nuno Vasconcelos. 2015. Scene Classification with Semantic Fisher Vectors. In *CVPR.*

[7] P. Dollár, R. Appel, S. Belongie, and P. Perona. 2014. Fast Feature Pyramids for Object Detection. *IEEE Transactions on Pattern Analysis and Machine Intelligence* 36, 8 (Aug 2014), 1532–1545. DOI: https://doi.org/10.1109/TPAMI.2014.2300479

[8] M. Everingham, L. Van Gool, C. K. I. Williams, J. Winn, and A. Zisserman. 2007. The PASCAL Visual Object Classes Challenge 2007 (VOC2007) Results. http://www.pascal-network.org/challenges/VOC/voc2007/workshop/index.html. (2007).

[9] R. Fan, K. Chang, C. Hsieh, X. Wang, and C. Lin. 2008. Liblinear: A library for large linear classification. *J. Mach. Learn. Res.* 9 (2008), 1871–1874.

[10] A. Farhadi, I. Endres, D. Hoiem, and D. A. Forsyth. 2009. Describing objects by their attributes. In *CVPR.*

[11] L. Fei-Fei and P. Perona. 2005. A bayesian hierarchical model for learning natural scene categories. In *CVPR.*

[12] P. F. Felzenszwalb, R. B. Girshick, D. McAllester, and D. Ramanan. 2010. Object Detection with Discriminatively Trained Part-Based Models. *IEEE Transactions on Pattern Analysis and Machine Intelligence* 32, 9 (Sept 2010), 1627–1645. DOI: https://doi.org/10.1109/TPAMI.2009.167

[13] Marian George, Mandar Dixit, Gábor Zogg, and Nuno Vasconcelos. 2016. *Semantic Clustering for Robust Fine-Grained Scene Recognition.* Springer International Publishing, Cham, 783–798. DOI: https://doi.org/10.1007/978-3-319-46448-0_47

[14] Ross Girshick. 2015. Fast R-CNN. In *The IEEE International Conference on Computer Vision (ICCV).*

[15] Ross Girshick, Jeff Donahue, Trevor Darrell, and Jitendra Malik. 2014. Rich Feature Hierarchies for Accurate Object Detection and Semantic Segmentation. In *The IEEE Conference on Computer Vision and Pattern Recognition (CVPR).*

[16] Y. Gong, L. Wang, R. Guo, and S. Lazebnik. 2014. Multi-scale orderless pooling of deep convolutional activation features. In *ECCV.*

[17] Saurabh Gupta, Pablo Arbelaez, Ross Girshick, and Jitendra Malik. 2014. Indoor scene understanding with RGB-D images: Bottom-up segmentation, object detection and semantic segmentation. *Int J Comput Vis* 112 (2014), 133–149.

[18] Saurabh Gupta, Pablo Arbeláez, Ross Girshick, and Jitendra Malik. 2015. Indoor Scene Understanding with RGB-D Images: Bottom-up Segmentation, Object Detection and Semantic Segmentation. *International Journal of Computer Vision* 112, 2 (2015), 133–149. DOI: https://doi.org/10.1007/s11263-014-0777-6

[19] S. Gupta, R. Girshick, P. Arbelaez, and J. Malik. 2014. Learning rich features from RGB-D images for object detection and segmentation. In *ECCV.*

[20] Saurabh Gupta, Judy Hoffman, and Jitendra Malik. 2016. Cross Modal Distillation for Supervision Transfer. In *The IEEE Conference on Computer Vision and Pattern Recognition (CVPR).*

[21] Mayank Juneja, Andrea Vedaldi, C. V. Jawahar, and Andrew Zisserman. 2013. Blocks that Shout: Distinctive Parts for Scene Classification. In *CVPR.*

[22] Christoph H. Lampert, Hannes Nickisch, and Stefan Harmeling. 2014. Attribute-Based Classification for Zero-Shot Visual Object Categorization. *IEEE Trans. on Image Process.* 36, 3 (2014), 453–465.

[23] Li-Jia Li, Hao Su, Yongwhan Lim, and Li Fei-Fei. 2014. Object Bank: An Object-Level Image Representation for High-Level Visual Recognition. *Int. J. Comput. Vision* 107, 1 (2014), 20–39. DOI: https://doi.org/10.1007/s11263-013-0660-x

[24] Xin Li and Yuhong Guo. 2014. Latent Semantic Representation Learning for Scene Classification. In *ICML.*

[25] Z. Niu, G. Hua, X. Gao, and Q. Tian. 2012. Context aware topic model for scene recognition. In *CVPR.*

[26] Genevieve Patterson, Chen Xu, Hang Su, and James Hays. 2014. The SUN Attribute Database: Beyond Categories for Deeper Scene Understanding. *Int. J. Comput. Vision* 108, 1-2 (2014), 59–81.

[27] Nikhil Rasiwasia and Nuno Vasconcelos. 2013. Latent Dirichlet Allocation Models for Image Classification. *IEEE Trans. on Pattern Anal. and Mach. Intell.* 35, 11 (2013), 2665–2679. DOI: https://doi.org/10.1109/TPAMI.2013.69

[28] Shaoqing Ren, Kaiming He, Ross Girshick, and Jian Sun. 2015. Faster R-CNN: Towards Real-Time Object Detection with Region Proposal Networks. In *Advances in Neural Information Processing Systems 28*, C. Cortes, N. D. Lawrence, D. D. Lee, M. Sugiyama, and R. Garnett (Eds.). Curran Associates, Inc., 91–99.

[29] J. Sanchez and F. Perronnin. 2011. High-Dimensional Signature Compression for Large-Scale Image Classification. In *Neural Comput.*

[30] Nathan Silberman, Derek Hoiem, Pushmeet Kohli, and Rob Fergus. 2012. Indoor Segmentation and Support Inference from RGBD Images. In *Proceedings of the 12th European Conference on Computer Vision - Volume Part V (ECCV'12).* Springer-Verlag, Berlin, Heidelberg, 746–760. DOI: https://doi.org/10.1007/978-3-642-33715-4_54

[31] J. Sivic, B. Russell, A. Efros, A. Zisserman, and W. Freeman. 2005. Discovering objects and their location in images. In *ICCV.*

[32] R. Socher, B. Huval, B. Bath, C. D. Manning, and A. Y. Ng. 2012. Convolutional-recursive deep learning for 3D object classification. In *NIPS.*

[33] Shuran Song, S. P. Lichtenberg, and Jianxiong Xiao. 2015. SUN RGB-D: A RGB-D scene understanding benchmark suite. In *Computer Vision and Pattern Recognition (CVPR), 2015 IEEE Conference on.* 567–576. DOI: https://doi.org/10.1109/CVPR.2015.7298655

[34] Xinhang Song, Luis Herranz, and Shuqiang Jiang. 2017. Depth CNNs for RGB-D Scene Recognition: Learning from Scratch Better than Transferring from RGB-CNNs. In *Proceedings of the Thirty-First AAAI Conference on Artificial Intelligence, February 4-9, 2017, San Francisco, California, USA.* 4271–4277.

[35] Xinhang Song, Shuqiang Jiang, and Luis Herranz. 2015. Joint Multi-Feature Spatial Context for Scene Recognition on the Semantic Manifold. In *The IEEE Conference on Computer Vision and Pattern Recognition (CVPR).*

[36] Xinhang Song, Shuqiang Jiang, Luis Herranz, Yan Kong, and Kai Zheng. 2016. Category co-occurrence modeling for large scale scene recognition. *Pattern Recognition* (2016), –. DOI: https://doi.org/10.1016/j.patcog.2016.01.019

[37] J. R. R. Uijlings, K. E. A. van de Sande, T. Gevers, and A. W. M. Smeulders. 2013. Selective Search for Object Recognition. *International Journal of Computer Vision* 104, 2 (2013), 154–171. DOI: https://doi.org/10.1007/s11263-013-0620-5

[38] Julia Vogel and Bernt Schiele. 2007. Semantic Modeling of Natural Scenes for Content-Based Image Retrieval. *Int. J. Comput. Vision* 72, 2 (April 2007), 133–157. DOI: https://doi.org/10.1007/s11263-006-8614-1

[39] Anran Wang, Jianfei Cai, Jiwen Lu, and Tat-Jen Cham. 2016. Modality and Component Aware Feature Fusion For RGB-D Scene Classification. In *The IEEE Conference on Computer Vision and Pattern Recognition (CVPR).*

[40] Jinjun Wang, Jianchao Yang, Kai Yu, Fengjun Lv, T. Huang, and Yihong Gong. 2010. Locality-constrained Linear Coding for image classification. In *CVPR.*

[41] Jianchao Yang, Kai Yu, Yihong Gong, and Thomas S. Huang. 2009. Linear spatial pyramid matching using sparse coding for image classification. In *CVPR.*

[42] Matthew D. Zeiler and Rob Fergus. 2014. Visualizing and Understanding Convolutional Networks. In *Computer Vision – ECCV 2014: 13th European Conference, Zurich, Switzerland, September 6-12, 2014, Proceedings, Part I.* Springer International Publishing, Cham, 818–833. DOI: https://doi.org/10.1007/978-3-319-10590-1_53

[43] Hongyuan Zhu, Jean-Baptiste Weibel, and Shijian Lu. 2016. Discriminative Multi-Modal Feature Fusion for RGBD Indoor Scene Recognition. In *The IEEE Conference on Computer Vision and Pattern Recognition (CVPR).*